CHEMISTRY OF MATERIALS
Article
Cite This: Chem. Mater. 2018, 30, 5655−5662
pubs.acs.org/cm

# Stabilizing Protic and Aprotic Liquid Electrolytes at High-Bandgap Oxide Interphases

Zhengyuan Tu,[†] Michael J. Zachman,[‡] Snehashis Choudhury,[§] Kasim A. Khan,[§] Qing Zhao,[§] Lena F. Kourkoutis,[‡,∥] and Lynden A. Archer*[,†,§]

[†]Department of Materials Science and Engineering, [‡]School of Applied and Engineering Physics, [§]Robert Frederick Smith School of Chemical and Biomolecular Engineering, and [∥]Kavli Institute at Cornell for Nanoscale Science, Cornell University, Ithaca, New York 14853, United States

Supporting Information

**ABSTRACT:** Approaches for regulating electrochemical stability of liquid electrolytes in contact with solid-state electrodes are a requirement for efficient and reversible electrical energy storage in batteries. Such methods are particularly needed in electrochemical cells in which the working potentials of the electrodes lie outside the thermodynamic stability limits of the liquid electrolyte. Here we study electrochemical stability of liquids at electrolyte/electrode interfaces protected by nanometer thick, high electrical bandgap ceramic phases. We report that well-designed ceramic *interphases* extend the oxidative stability limits for both protic and aprotic liquid electrolytes, in some cases by as much as 1.5 V. It is shown further that such interphases facilitate stable electrodeposition of reactive metals such as lithium at high Coulombic efficiency and in electrochemical cells subject to extended galvanostatic cycling at a current density of 3 mA cm$^{-2}$ and at capacities as high as 3 mAh cm$^{-2}$. High-resolution cryo-FIB-SEM characterization reveals that solid/compact Li electrodeposits anchored by the ceramic interphase are the source of the enhanced Li deposition stability. The results enable a proof-of-concept "anode-free" Li metal rechargeable battery in which Li initially provided in the cathode is the only source of lithium in the cell.

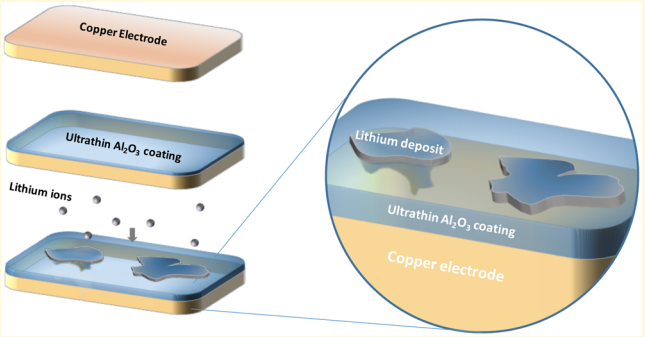


## INTRODUCTION

Rechargeable batteries are designed to reversibly convert stored chemical energy to electricity and are of interest in a growing number of applications, including portable electronics, electric vehicles, and renewable energy storage.[1−4] To meet increasing demand for reliable, safe, and more energy dense storage, attention has turned to understanding and controlling nanoscale physical and chemical processes at the solid electrode/liquid electrolyte and solid electrode/solid electrolyte interphases that normally form spontaneously during the first cycles of battery operation.[5,6] The chemical composition, thickness, structure, and transport properties of these interphases are now understood to be key determinants of battery performance and lifetime, but because of the complexity of spontaneously formed interphases, little is known about how and why each of these variables impacts cell-level performance, and even less is known about how they might be rationally designed to achieve a desired electrochemical function. It is remarkable, for example, that although the chemical potential (Fermi level) of the graphitic carbon anode in a lithium-ion battery (LIB) lies well above the lowest unoccupied molecular orbital (LUMO) of widely used aprotic liquid electrolytes, LIBs can be operated stably for hundreds to thousands of charge/discharge cycles at high Coulombic efficiencies. The expectation that widely used alkyl carbonate electrolytes would undergo continuous reduction when in contact with the graphitic anode in state-of-the art LIBs is proven false largely as a result of the robust, electrochemically stable, and self-limiting solid electrolyte interphase (SEI) layer formed spontaneously on the anode by electrochemical breakdown of electrolyte components.[7] We note that these issues are also pronounced at interfaces between solid-state electrolytes and battery anodes[8] as well as between emerging high voltage nickel-rich intercalation cathodes and liquid electrolytes.[9]

A well-formed and stable SEI is even more critical for emergent metal anode based rechargeable batteries, where the graphitic carbon anode of LIBs is replaced by more electrochemically active elements such as Li, Na, Si, and Sn to achieve higher energy density.[10,11] In addition to the electrochemical stability of the electrolyte at the anode working potential, the intrinsic high Fermi levels of Li and Na means that even in the rest state, there is a thermodynamic driving force that favors continuous reduction of electrolyte in contact

Received: May 16, 2018
Revised: July 24, 2018
Published: July 25, 2018






DOI: 10.1021/acs.chemmater.8b01996
Chem. Mater. 2018, 30, 5655−5662

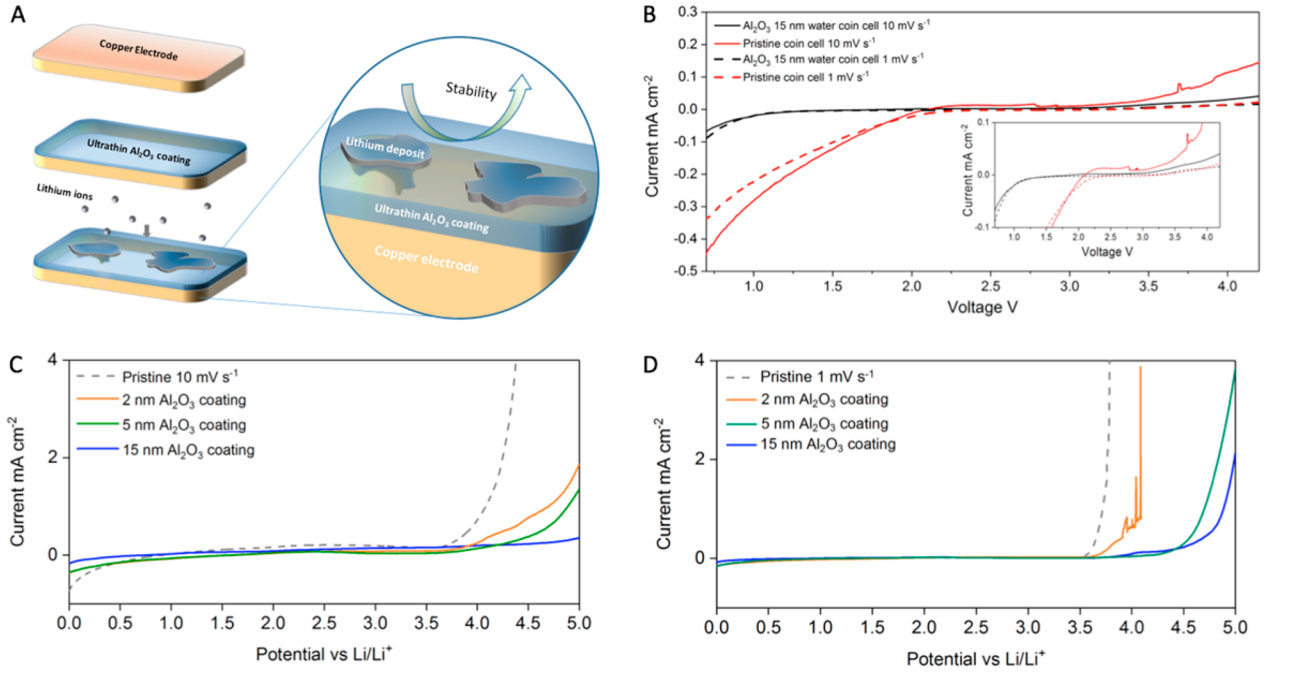


**Figure 1.** (A) Schematic illustration of the ultrathin oxide (e.g., $Al_2O_3$) artificial SEI on a conductive substrate. (B) Electrochemical stability test of the $Al_2O_3$ coated interphase from −1.8 to 1.8 V vs stainless steel at various potential sweeping rates in 1 M LiTFSI/water. (C) Electrochemical stability test Li−$Al_2O_3$ Cu cells with 2, 5, and 15 nm thickness and control from 0 to 5 V vs $Li/Li^+$ at 10 mV $s^{-1}$ in 1 M $LiPF_6$/PC. (D) Electrochemical stability test of Li−$Al_2O_3$ Cu cells with 2, 5, and 15 nm thickness and control from 0 to 5 V vs $Li/Li^+$ at 1 mV $s^{-1}$ in 1 M $LiPF_6$/PC.

with the metals. In addition, these parasitic reactions between active metal anodes and electrolytes are now understood to be the root cause of many failure modes, including voltage divergence, dendrite formation via morphological instability, and active electrode material loss.[12] Even more problematic is the fact that the electroplating and alloying reactions these metals undergo during battery charge result in rather large volume changes (as high as 250% for a Sn anode).[13] This means that a spontaneously formed SEI must not only possess the traits theorized for the success of the SEI in LIBs—self-limiting formation, electronically insulating, and ionically conductive—but must also be able to flex and stretch to accommodate volume changes at the electrode without cracking or structural breakdown.

Herein, we report on the physical properties, electrochemical features, and stability of what we here term model artificial solid−electrolyte interphases (ASEI) created from ultrathin conformal ceramic coatings, which allow us to investigate the electrochemical stability of liquid electrolytes at both high and low potentials. The hypothesis that guides the study is that by excluding ions and electrolyte solvent from regions near a charged surface where the electrical potential is greatest and varies most strongly with distance from the electrode, a uniform, high electrical bandgap coating on the electrode would lower the electric field and field-induced forces on all species in an electrolyte, enhancing electrochemical stability at the interface. Figure 1A illustrates the configuration of the electrodes and ASEI used in this study. A key finding is that even at thicknesses as low as 15 nm, liquid electrolytes in contact with such interphases display very large increases in anodic and cathodic stability. As illustrated in Figure 1B−D, the improvements in electrolyte stability are realized in both protic and aprotic liquids. Results reported in Figure 1B, for example, show that an ASEI composed of a 15 nm thick $Al_2O_3$ ALD coating on a stainless steel electrode increases the electrochemical stability window of an aqueous 1 M LiTFSI electrolyte by more than 1.5 V. Adopting a $Li/Li^+$ reference reveals that the voltage stability range achieved is 1.1−4.2 V ($Li/Li^+$), which is comparable to results reported in recent pioneering studies using so-called water-in-salt electrolytes composed of 21 M LiTFSI.[14] Application to aprotic liquid electrolytes composed of 1 M $LiPF_6$ in propylene carbonate (PC) shows that both the electrochemical stability and ability of the electrolyte to sustain stable and reversible electrodeposition of Li metal are enhanced significantly, underscoring the importance of the anode/electrolyte interphase in stabilizing Li and other reactive metal anodes prone to fail by rough, dendritic depositions and parasitic reactions with liquid electrolytes. By combining the $Al_2O_3$ ASEI with a suitable liquid electrolyte, we further show that it is possible to achieve high-Coulombic efficiency (>98%) and stable lithium cycling at a current density as high as 3 mA $cm^{-2}$. Building on these observations, we investigate long-term stability in so-called anode free lithium cells where the only source of Li is in the cathode.

A variety of approaches have been proposed in the literature for fabricating electrolyte/electrode interphases that achieve a specific electrochemical function, e.g., extended electrochemical stability,[15,16] passivation of a reactive anode against parasitic chemical reactions with an electrolyte,[17,18] formation of compact dendrite-free deposition of metals such as Li and Na during battery recharge,[19,20] and so forth. The vast majority of these designs rely on preferential degradation of so-called SEI forming molecular additives, such as ethylene carbonate, vinylene carbonate, fluorinated compounds, etc., which are introduced as sacrificial agents in an electrolyte.[21−24] Achieving interphases with favorable composition, structure, and physical properties therefore requires extensive trial-and-error exper-


DOI: 10.1021/acs.chemmater.8b01996
Chem. Mater. 2018, 30, 5655−5662

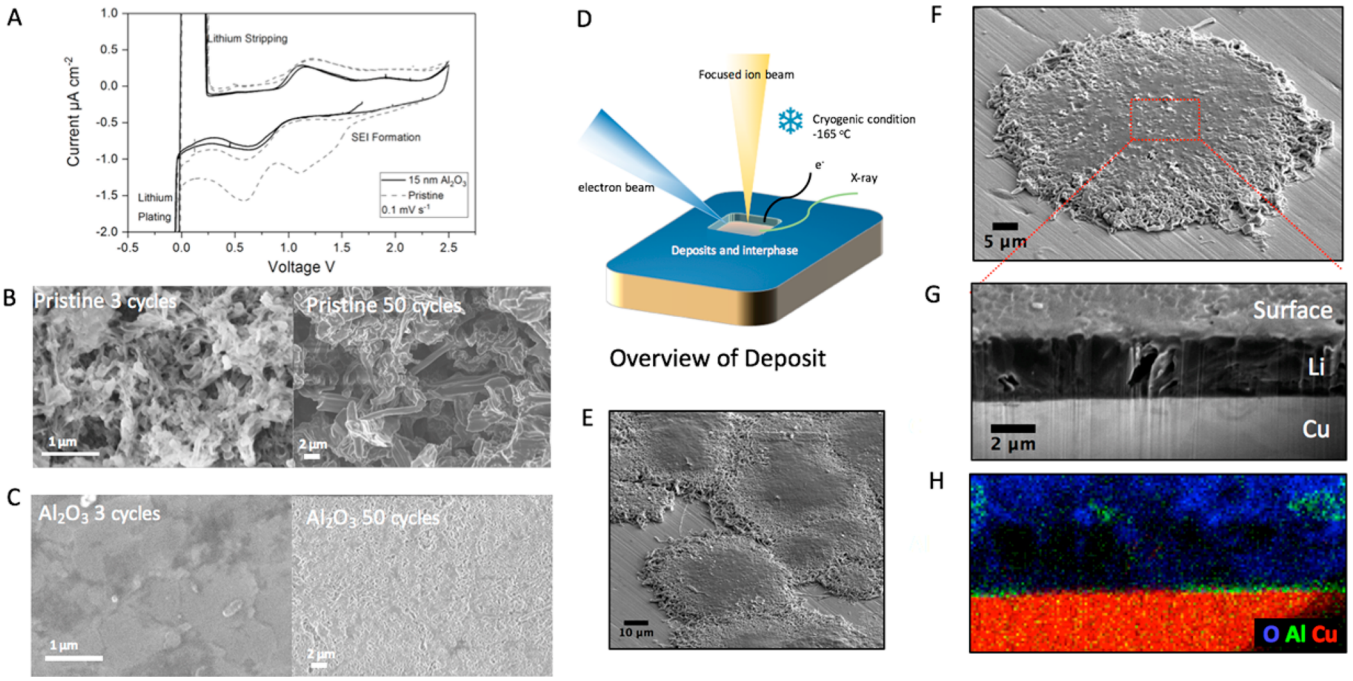


**Figure 2.** (A) Cyclic voltammogram of the Li−Cu asymmetric cell with/without 15 nm thick $Al_2O_3$ coating in 1 M $LiPF_6$/PC scanned at 0.1 mV $s^{-1}$. (B) Postmortem SEM images of the bare interphase after 3 and 100 cycles in 1 M $LiPF_6$/PC. (C) Postmortem SEM images of the 15 nm thick $Al_2O_3$ interphase after 3 and 100 cycles in 1 M $LiPF_6$/PC. (D) An illustration of the cryo-FIB-SEM setup at liquid nitrogen temperature. (E) A cryo-FIB-SEM overview of deposits on the 15 nm thick $Al_2O_3$-coated interphase. (F) Zoom-in view of a deposit before cryo-FIB-SEM milling, with red rectangle highlighting the milled region. (G) Cross-sectional image of an electrodeposit on a 15 nm thick $Al_2O_3$-coated interphase. (H) EDX elemental mapping of the cross section shown in (G).

imentation.[25,26] While these approaches have been successful in creating intermediate voltage LIBs with exceptional stability and efficiency, their effectiveness in achieving stability of electrochemically active metal electrodes has been less impressive. A more promising approach is to select the electrolyte solvent itself for its ability to produce mechanically robust interphases. In this regard, ether- and ester-based electrolytes have been actively investigated for their ability to form stable and conductive SEI that facilitates reversible lithium plating/stripping during extended cycling.[27] Concerns about the narrow electrochemical stability window of such electrolyte solvents and their potential for gas formation during battery cycling have, until recently, been a major drawback.[6] These concerns have been partially alleviated by demonstrations of markedly enhanced electrochemical stability windows of liquid electrolytes containing large concentrations of soluble salts.[28] Unfortunately, salts with the required levels of stability and solubility are expensive and incompatible with solid-state, polymer versions of these electrolytes, which raises additional concerns about the practicality of the proposed solution.[28]

ASEI based on preformed materials, including polymer thin films, particles of various sorts, solid-state electrolytes, two-dimensional materials, and so on, present a viable alternative to solution-based methods. Interphases based on these materials have been prepared by casting, vapor deposition, layer-by-layer assembly, or direct reaction of components on metal electrodes.[15,19,29−32] With few exceptions,[18,30] achieving conformal coatings of uniform thickness at the requisite electrode/electrolyte interfaces is challenging, and success is largely determined on a case-by-case basis. Solid-state electrolytes including various ion conductive polymers and ceramics are widely believed to maintain morphological stability of the metal/electrolyte interface in metal-based rechargeable batteries. However, the poor contact between the solid electrode and electrolyte has emerged as a serious limitation to progress, and strategies for lowering the interfacial resistance to facilitate room temperature cell operation are an area of significant recent activity.[8] Here we find that atom-by-atom deposition of the ASEI by means of atomic layer deposition (ALD) provides a straightforward strategy for creating ultrathin ceramic coatings on metals that overcome these limitations.

## RESULTS AND DISCUSSION

The results in Figure 1B−D show that the improved stability observed upon application of the ASEI is insensitive to the voltage scan rate (linear scan measurements at 10 and 1 mV $s^{-1}$ reveal at most minor changes in stability), confirming that the effect is not merely the result of impeded ion transport to the interface. For a 1 M $LiPF_6$−PC electrolyte between Li and $Al_2O_3$/Cu electrodes with various $Al_2O_3$ coating thicknesses, the results in Figure 1C,D further show that there is a progressive increase of the cathodic stability as the thickness of the $Al_2O_3$ coating increases. Note that the baseline currents are at the same level for systems with various coating thickness, as shown in Figure S1, excluding the artifact of lowered current from increased impedance. Specifically, whereas the control cell without the $Al_2O_3$ ASEI is seen to exhibit a current divergence at around 3.6 V, possibly due to the known Cu corrosion in this range of voltage, the Li−15 nm thick $Al_2O_3$/Cu cells manifest negligible current until around 4.7 V, even at a slow scan rate of 1 mV $s^{-1}$ when ample time is allowed for transport and decomposition reactions at solid/liquid interfaces, clearly demonstrating that an $Al_2O_3$ ASEI with desirable


DOI: 10.1021/acs.chemmater.8b01996
Chem. Mater. 2018, 30, 5655−5662

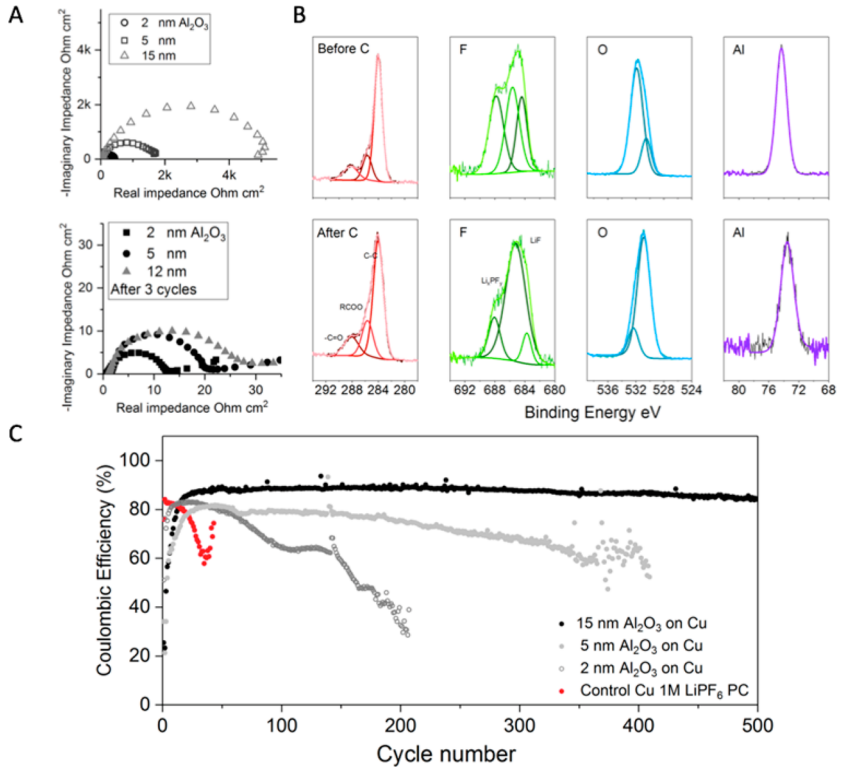


**Figure 3.** (A) Impedance spectra of the $Al_2O_3$-coated interphase with different thicknesses in 1 M $LiPF_6$/PC (top) and after three charge/discharge cycles (bottom). (B) High-resolution XPS spectra of the 15 nm thick $Al_2O_3$-coated interphase before and after cycling. (C) Coulombic efficiency measurement of the $Al_2O_3$-coated interphase with different thicknesses operated at 1 mA $cm^{-2}$ for 0.5 mAh $cm^{-2}$ capacity per cycle.

thickness can profoundly extend the high-voltage stability of all components (solvent and salt) in a liquid electrolyte.

Figure 2A compares cyclic voltammograms of Li−Cu and Li−$Al_2O_3$/Cu from 2.5 to −0.2 V at a scan rate of 0.1 mV $s^{-1}$. In both cases, the peaks from −0.2 to 0.2 V show typical metal deposition and stripping characteristics, indicating that reversible lithium cycling is not hindered by the $Al_2O_3$ coating (Figure S2). Cathodic peaks between 0.5 and 0.7 V are also observed in cells with and without $Al_2O_3$ coating along with their corresponding anodic peaks starting from 1 V, indicating a reversible process likely related to the SEI forming/reforming process related to propylene carbonate.[31] However, a pronounced difference can be observed during the first discharge: prior to the lithium plating, a broad peak in the range 1−1.5 V is observed in the pristine cell, typically associated with decomposition of the electrolyte[3] and impurities, which is completely prevented with the application of a 15 nm thick $Al_2O_3$ coating. In other words, the results show that the natural formation of a poor quality SEI can be arrested by with the interphase $Al_2O_3$ in the conventionally used liquid electrolytes. The $Al_2O_3$ ASEI is also found to drastically improve the lithium deposition morphology, as in Figure 2B,C showing the top-view morphology of locations where the electrodeposition occurs. Propylene carbonate has been known to form an insulating and fragile SEI, which produces low Coulombic efficiency in rechargeable lithium batteries.[33] Figure 2B shows that the poor SEI also adversely affects electrode morphology by promoting uneven electrodeposition of lithium, which evolves to a dendritic structure after multiple cycles. Contrarily, as seen in Figure 2C, a 15 nm thick $Al_2O_3$ coating yields compact and dendrite-free Li electrodeposits.

To determine the mechanism by which the $Al_2O_3$ ASEI enhances interfacial stability, we employed cryo-focused ion beam scanning electron microscopy (cryo-FIB-SEM) (Figure 2D) to characterize the morphology and structure of the lithium deposits. Cryo-FIB-SEM enables high-quality cross-sectional images of lithium deposits to be obtained, which are not achievable with conventional room temperature FIB approaches due to the tendency of materials such as lithium to react with the ions used during milling. Figure 2E reports a typical cryo-FIB-SEM image of a 15 nm thick $Al_2O_3$/Cu electrode in 1 M $LiPF_6$/PC after three cycles of charge and discharge before milling. It is apparent that the lithium deposits form a complex structure in which very large island-like satellites are connected to a compact, flat center by fibrous edges. Cryo-FIB-SEM milling allows the cross-sectional morphology of the deposits to be scrutinized, as shown in Figure 2F−H. It is seen that a dense layer of lithium with a thickness of ≈3 $\mu$m exists at the center of the deposits and that the edges are composed of a relatively loose, rough structure. These results are to our knowledge the first demonstration that Li can form solid dense electrodeposits in liquid electrolytes. Energy-dispersive X-ray spectroscopy (EDX) mapping was employed to elucidate the chemistry of the cross section of the material. The results show local devoid of oxygen confirming the existence of electrodeposited lithium, which is not detectable in our EDX setup. A portion of $Al_2O_3$ in the middle of the map appears to be lifted off of the copper surface, allowing Li deposition beneath the $Al_2O_3$ ASEI, though the majority of the Li mass is actually on top of the $Al_2O_3$ coating surrounding this point. Considering that $Al_2O_3$ is an electrical insulator, this unorthodox result may be explained by radial growth of the lithium deposit under the



DOI: 10.1021/acs.chemmater.8b01996
Chem. Mater. 2018, 30, 5655−5662

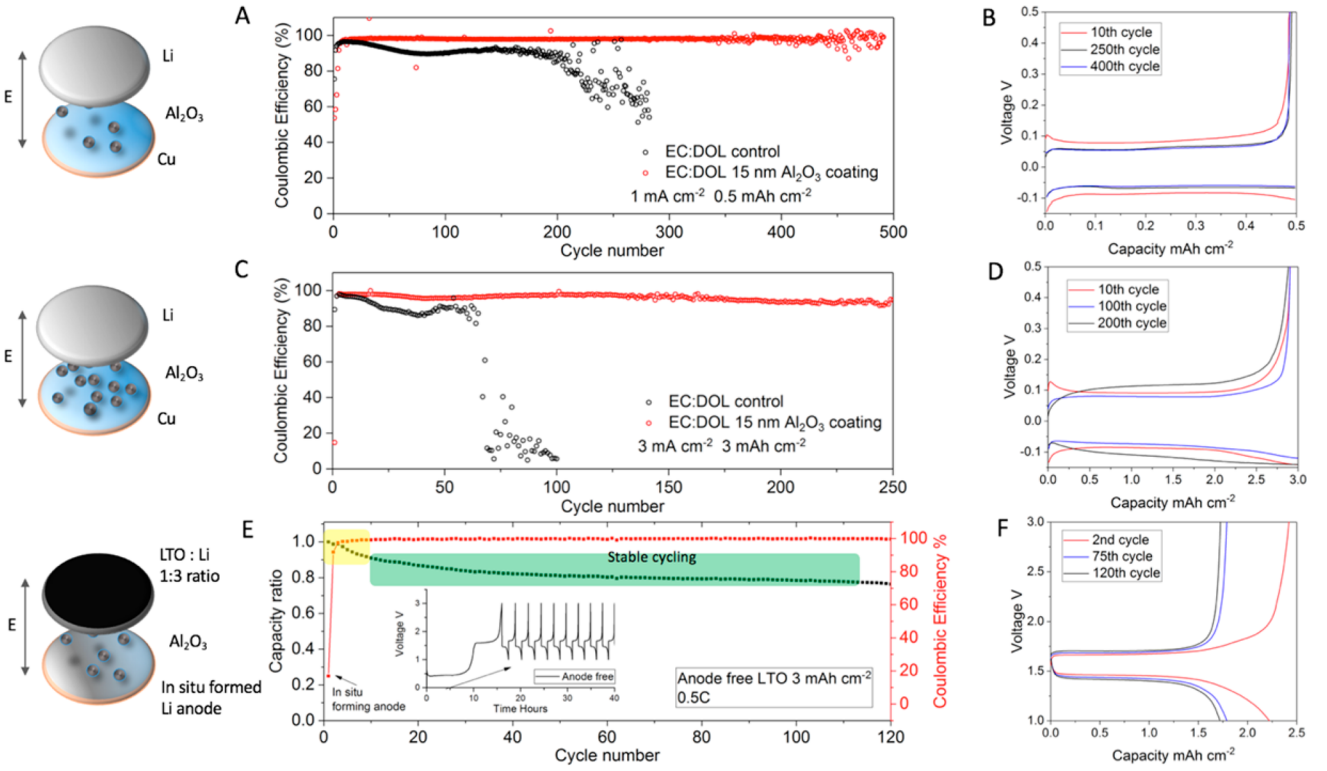


**Figure 4.** (A) Coulombic efficiency measurement of the 15 nm thick $Al_2O_3$-coated interphase and bare interphase in 1 M $LiPF_6$/EC:DOL (9:1 vol %) at a current density of 1 mA $cm^{-2}$ and capacity of 0.5 mAh $cm^{-2}$, with the illustration on the left. (B) Voltage−areal capacity profile at different cycles for part A. (C) Coulombic efficiency measurement of the 15 nm thick $Al_2O_3$-coated interphase and bare interphase in 1 M $LiPF_6$/EC:DOL (9:1 vol %) at a current density of 3 mA $cm^{-2}$ and capacity of 3 mAh $cm^{-2}$. (D) Voltage−areal capacity profile at different cycles for part C. (E) Anode-free model cell with lithium originating in the LTO counter electrode (capacity of LTO:Li = 1:3) operated at 0.5 C with the lithium anode formed in situ during the first cycle (inset). (F) Voltage−areal capacity profile at different cycles for part E.

strained ASEI from the center of the island outward, as confirmed by further cryo-FIB-SEM images and EDX mapping of multiple electrodeposits formed at a low current density (Figures S3 and S4). We conclude, therefore, that the $Al_2O_3$ layer essentially serves to anchor the Li deposit to the current collector, which ensures good adhesion between the lithium deposit mass and current collector, facilitating good electronic transport through the Li mass and facilitating uniform deposition.

Impedance spectroscopy provides additional insights into the behavior of the $Al_2O_3$ surface layer in an electrochemical system. Figure 3A reports the impedance spectra of the Li−$Al_2O_3$/Cu asymmetric cell as a function of $Al_2O_3$ coating thickness in the range 2−15 nm. Results in the figure show that the interfacial impedance increases with coating thickness. This trend continues with further increases in the coating thickness, as demonstrated in Figure S5. Figure 3A also shows that while the trend of increasing interfacial impedance with increasing $Al_2O_3$ thickness is preserved after cycling the Li−$Al_2O_3$/Cu asymmetric cells, the interfacial impedance of cells with higher $Al_2O_3$ thickness decreases by several orders of magnitude, with the result that the area specific resistance (ASR) at all coating thicknesses is low. This large reduction in interfacial resistance could arise from lithiation of the $Al_2O_3$ coatings and/or from stress-induced cracks in the coating, which would facilitate direct contact with the liquid electrolyte. The latter hypothesis can be partially ruled out by the fact that the interfacial impedance remains a strong function of coating thickness. To more thoroughly evaluate the two hypotheses, X-ray photoelectron spectroscopy (XPS) was employed to elucidate the surface chemistry of $Al_2O_3$/Cu electrode before and after lithium electrodeposition, as reported in Figure 3B. The carbon spectra and their decoupled components (C−H 284.1 eV, C−O 285.5 eV, and C═O 288.3 eV) remain virtually unchanged after lithium electrodeposition, confirming that minimal decomposition of the PC-based electrolyte occurs, which is inconsistent with expectations for the ASEI cracking mechanism. A variation of the fluorinated species is observed as indicated by the forming $LiP_xF_y$ and LiF, likely from the breakdown of the salt. The aluminum signal remains pronounced after cycling, despite a reduced intensity likely related to the surface masked by electrodeposits. The aluminum peak also exhibits a negative shift in the binding energy from 74.4 eV, which is typical for $Al_2O_3$, to 73.5 eV. Such change is believed to be associated with the lithiation and the reduction of the $Al_2O_3$ upon the interaction of lithium, as also confirmed by the slight negative shift from the deconvoluted oxygen peaks.[34] XPS results confirms the effectiveness of $Al_2O_3$ coating arises from generating and maintaining a stable and conductive SEI upon cycling.

The $Al_2O_3$ coating also has a major influence on the Coulombic efficiency (CE) of lithium plating/stripping. Figure 3C compares the CE of Li−Cu and Li−$Al_2O_3$ Cu asymmetric cells cycled in 1 M $LiPF_6$ PC at a current density of 1 mA $cm^{-2}$ for 0.5 mAh $cm^{-2}$ capacity, with different $Al_2O_3$ coating thicknesses. The lithium electrodeposition on the bare Cu is observed to occur at low CE, which quickly decreases in the first 50 cycles, a result within our expectation as PC is known to form a poor SEI which results in low efficiency stripping and plating of Li. In contrast, both CE values and the lifetime


DOI: 10.1021/acs.chemmater.8b01996
Chem. Mater. 2018, 30, 5655−5662

before failure are markedly improved with thicker $Al_2O_3$ coating with the same liquid electrolyte used in all cells. The 15 nm thick $Al_2O_3$ coating provides what appears to be the optimal CE ≈ 90% over 500 cycles (Figure S6) with only a small increase in overpotential—an impressive result for a PC-based electrolyte. Further increasing the thickness of the coating does not contribute to better performance, likely due to the insulating nature of $Al_2O_3$. The result can be trivially explained in terms of the $Al_2O_3$ ASEI protection of Li against parasitic side reactions. The high bandgap of $Al_2O_3$ (~7 eV) likely alters the voltage profile in the vicinity of the electrode and thus slows down the decomposition of PC, implied by results from same experiments on asymmetric cells with $HfO_2$ and $TiO_2$ (Figure S7)—two materials with lower bandgaps of ~5.5 and 3.2 eV, respectively. More detailed investigation of the lithium electrodeposition process, however, suggests that this explanation is incomplete. Specifically, by combining the morphological and electrochemical analytical studies, we believe that a "lifting−expanding−jointing" process is involved during the electrodeposition, which exposes the edge of the deposits to the electrolyte. That means the lifting of the $Al_2O_3$ creates the space for the further electrodeposition of Li, which expands horizontally until joining with other electrodeposits. The enhanced stability provided by the $Al_2O_3$ coating therefore appears to stem primarily from the protection provided by the $Al_2O_3$ overlayer and the strong adhesion achieved near the deposit nucleus (root) and the current collector, which also limits the formation of electronically disconnected or "dead" lithium.

Additional support for this mechanism comes from electrochemical studies in a EC:DOL-based electrolyte that exhibit greater chemical stability in contact with Li. Similar to the PC-based electrolyte, the natural decomposition of the solvent and impurities can be prevented, as shown in Figure S8. Figures 4A and 4C report results from CE measurements using control Li−Cu and Li−15 nm $Al_2O_3$ Cu asymmetric cells cycled in a 1 M $LiPF_6$ EC:DOL electrolyte at different current densities and capacities. The control cells exhibit initial CE > 95%, but the values quickly decrease, with clear signs of interphase failure after 200 cycles at 1 mA $cm^{-2}$ for 0.5 mAh $cm^{-2}$ and 50 cycles at 3 mA $cm^{-2}$ for 3 mAh $cm^{-2}$. In contrast, the Li−15 nm $Al_2O_3$ Cu cells exhibit high and stable CE > 98% even at a high current density and capacity for over 250 cycles without any obvious signs of failure. Voltage−capacity profiles provided in Figures 4B and 4D show that the cells cycle with minimal overpotential buildup, indicative that the interface is stable. The higher overpotential after 10 cycles at a high current density can be attributed to the nucleation of lithium electrodeposits in the first few cycles. The high CE achieved with this combination of ASEI and electrolyte can be tested more rigorously in a so-called *anode-free* lithium battery, in which an overlithiated or thick cathode is the only source of Li in the cell and the anode used in the cycling studies is formed in situ by lithium deposition on a $Al_2O_3$ Cu current collector during the first cycle. As a demonstration of the concept, cells with a 15 nm thick $Al_2O_3$ Cu-LTO (areal capacity 3 mAh $cm^{-2}$) configuration were constructed with a thin lithium foil placed on the LTO electrode to mimic an overlithiated cathode. The capacity ratio between the Li in the overlayer and Li in the LTO electrode was maintained as 3 to 1. The initial voltage profile measured in the first charge cycle is illustrated in the inset of Figure 4E. A clear long first charge step with two voltage plateaus which represent the lithium deposition under low potential (~0.4 V for Li−Li) and high potential (1.5 V for LTO−Li) is observed. At the point of transition, it can be seen from the voltage profiles that the cell performs identically to a typical Li−LTO cell. Stable, high CE charge−discharge cycling is achieved for over 120 cycles, which compares well to what is observed for the Cu−LTO control cell in the same electrolyte, where by the 10th cycle (Figures S9 and S10) the initial capacity is already below 80% of the initial value. The stable battery cycling performance is attributed to the high Coulombic efficiency of $Al_2O_3$ Cu−LTO cell, as directly calculated from the equation $R_{np}(CE)^n = 80\%$, in which $R_{np}$ represents the N/P capacity ratio, CE is the average Coulombic efficiency and $n$ is the cycle number before 80% capacity retention. The $Al_2O_3$ Cu−LTO cell thus exhibits an average CE of 98.9%, whereas the cell without artificial SEI shows a CE of about 91%. $Al_2O_3$ deposition also enables high-voltage LMB as tested in prototype cells with the $LiNi_{0.6}Co_{0.2}Mn_{0.2}O_2$ (NCM 622) cathode in which the N/P capacity ratio is kept about 3 to 1. To avoid the phase transition of NCM electrode upon direct contact with lithium, lithium is predeposited on the $Al_2O_3$ Cu to form the anode. Figures S11 and S12 report the reasonably well cycling and voltage profile of the thin Li−NCM cell showing a CE of about 96.7%. Together with the LTO cell results, it is testified that a rationally designed artificial interphase of ALD $Al_2O_3$ leads to promising application of practical LMB.

## CONCLUSIONS

To summarize, we show that by facilely engineering the electrode/electrolyte interphase with a pinhole-free few nanometer thick $Al_2O_3$ coating, it is possible to dramatically improve the electrochemical stability of protic and aprotic liquid electrolytes. At low voltages, the $Al_2O_3$ layer also serves as an effective artificial SEI which enables long-term reversible and efficient lithium cycling even in a poor SEI-forming propylene carbonate electrolyte. The ASEI is shown to promote formation of flat, compact Li electrodeposits that maintain strong attachment to the Cu current collector and appear to grow by a "lifting−expanding−jointing" process. By incorporating a new, high-efficiency (EC−DOL) electrolyte design, the $Al_2O_3$ ASEI is reported to yield stable high-efficiency lithium plating/stripping with a CE > 98% at a current density of 3 mA $cm^{-2}$ and a capacity of 3 mAh $cm^{-2}$ for over 250 cycles. We take advantage of these results to demonstrate in situ formation of Li anodes and stable charge/discharge cycling of so-called anode-free lithium metal cells in which an overlithiated LTO cathode with a 3 to 1 lithium−cathode capacity ratio is the only source of Li in the cell. Our observations are consistent with previous findings reported in ref 16 that spontaneously formed interphases based on hairy $SiO_2$ nanoparticle additives in liquid electrolytes enhance the electrochemical stability limits of liquids. They are also consistent with results provided in the Supporting Information, which show that nano-sized $Hf_2O$ electrode coatings (a material of intermediate electrical bandgap) created using ALD enable higher CE cycling of Li anodes.

## ASSOCIATED CONTENT

### Supporting Information

The Supporting Information is available free of charge on the ACS Publications website at DOI: 10.1021/acs.chemmater.8b01996.



DOI: 10.1021/acs.chemmater.8b01996
*Chem. Mater.* 2018, 30, 5655−5662

Detailed experimental description, SEM, EDX, and electrochemical characterization (PDF)

## AUTHOR INFORMATION


### Corresponding Author

*E-mail: laa25@cornell.edu (L.A.A.).

### ORCID

Zhengyuan Tu: 0000-0002-7291-6144

Lynden A. Archer: 0000-0001-9032-2772


### Author Contributions

Z.T. and M.J.Z. contributed equally to this work.

### Notes

The authors declare no competing financial interest.

## ACKNOWLEDGMENTS

This work was supported by the Department of Energy, Advanced Research Projects Agency-Energy (ARPA-E), through Award #DE-AR0000750. M.J.Z. and L.F.K. acknowledge support by the NSF (DMR-1654596). The work made use of electrochemical characterization facilities in the KAUST-CU Center for Energy and Sustainability, supported by the King Abdullah University of Science and Technology (KAUST) through Award # KUS-C1-018-02. This work made use of the Cornell Center for Materials Research (CCMR) Shared Facilities which are supported through the NSF MRSEC program (DMR-1719875). Additional support for the FIB/SEM cryo-stage and transfer system was provided by the Kavli Institute at Cornell and the Energy Materials Center at Cornell, DOE EFRC BES (DE-SC0001086).

## REFERENCES


(1) Tarascon, J. M.; Armand, M. Issues and challenges facing rechargeable lithium batteries. *Nature* **2001**, *414*, 359−367.

(2) Armand, M.; Tarascon, J. M. Building better batteries. *Nature* **2008**, *451*, 652−657.

(3) Etacheri, V.; Marom, R.; Elazari, R.; Salitra, G.; Aurbach, D. Challenges in the development of advanced Li-ion batteries: a review. *Energy Environ. Sci.* **2011**, *4*, 3243−3262.

(4) Yoshino, A. The Birth of the Lithium-Ion Battery. *Angew. Chem., Int. Ed.* **2012**, *51*, 5798−5800.

(5) Cheng, X. B.; Zhang, R.; Zhao, C. Z.; Wei, F.; Zhang, J. G.; Zhang, Q. A review of solid electrolyte interphases on lithium metal anode. *Adv. Sci.* **2016**, *3*, 1500213.

(6) Xu, K. Electrolytes and interphases in Li-ion batteries and beyond. *Chem. Rev.* **2014**, *114*, 11503−11618.

(7) Verma, P.; Maire, P.; Novák, P. A review of the features and analyses of the solid electrolyte interphase in Li-ion batteries. *Electrochim. Acta* **2010**, *55*, 6332−6341.

(8) Manthiram, A.; Yu, X.; Wang, S. Lithium battery chemistries enabled by solid-state electrolytes. *Nat. Rev. Mater.* **2017**, *2*, 16103.

(9) Edström, K.; Gustafsson, T.; Thomas, J. O. The cathode−electrolyte interface in the Li-ion battery. *Electrochim. Acta* **2004**, *50*, 397−403.

(10) Lin, D.; Liu, Y.; Cui, Y. Reviving the lithium metal anode for high-energy batteries. *Nat. Nanotechnol.* **2017**, *12*, 194−206.

(11) Tu, Z.; Nath, P.; Lu, Y.; Tikekar, M. D.; Archer, L. A. Nanostructured electrolytes for stable lithium electrodeposition in secondary batteries. *Acc. Chem. Res.* **2015**, *48*, 2947−2956.

(12) Tikekar, M. D.; Choudhury, S.; Tu, Z.; Archer, L. A. Design principles for electrolytes and interfaces for stable lithium-metal batteries. *Nat. Energy* **2016**, *1*, 16114.

(13) Hu, R.; Zhu, M. Sn-Based Alloy Anode Materials for Lithium-Ion Batteries: Preparation, Multi-scale Structure, and Performance. In *Nanomaterials in Advanced Batteries and Supercapacitors*; Springer: 2016; pp 93−125.

(14) Suo, L.; Borodin, O.; Gao, T.; Olguin, M.; Ho, J.; Fan, X.; Luo, C.; Wang, C.; Xu, K. Water-in-salt" electrolyte enables high-voltage aqueous lithium-ion chemistries. *Science* **2015**, *350*, 938−943.

(15) Li, J.; Dudney, N. J.; Nanda, J.; Liang, C. Artificial solid electrolyte interphase to address the electrochemical degradation of silicon electrodes. *ACS Appl. Mater. Interfaces* **2014**, *6*, 10083−10088.

(16) Choudhury, S.; Agrawal, A.; Wei, S.; Jeng, E.; Archer, L. A. Hybrid Hairy Nanoparticle Electrolytes Stabilizing Lithium Metal Batteries. *Chem. Mater.* **2016**, *28*, 2147−2157.

(17) Li, N. W.; Yin, Y. X.; Yang, C. P.; Guo, Y. G. An artificial solid electrolyte interphase layer for stable lithium metal anodes. *Adv. Mater.* **2016**, *28*, 1853−1858.

(18) Tu, Z.; Choudhury, S.; Zachman, M. J.; Wei, S.; Zhang, K.; Kourkoutis, L. F.; Archer, L. A. Designing Artificial Solid-Electrolyte Interphases for Single-Ion and High-Efficiency Transport in Batteries. *Joule* **2017**, *1*, 394.

(19) Ma, L.; Kim, M. S.; Archer, L. A. Stable artificial solid electrolyte interphases for lithium batteries. *Chem. Mater.* **2017**, *29*, 4181−4189.

(20) Wei, S.; Choudhury, S.; Xu, J.; Nath, P.; Tu, Z.; Archer, L. A. Highly Stable Sodium Batteries Enabled by Functional Ionic Polymer Membranes. *Adv. Mater.* **2017**, *29*, 1605512.

(21) Lu, Y.; Tu, Z.; Archer, L. A. Stable lithium electrodeposition in liquid and nanoporous solid electrolytes. *Nat. Mater.* **2014**, *13*, 961−969.

(22) Lu, Y.; Tu, Z.; Shu, J.; Archer, L. A. Stable lithium electrodeposition in salt-reinforced electrolytes. *J. Power Sources* **2015**, *279*, 413−418.

(23) Ding, F.; Xu, W.; Graff, G. L.; Zhang, J.; Sushko, M. L.; Chen, X.; Shao, Y.; Engelhard, M. H.; Nie, Z.; Xiao, J.; et al. Dendrite-free lithium deposition via self-healing electrostatic shield mechanism. *J. Am. Chem. Soc.* **2013**, *135*, 4450−4456.

(24) Lee, Y. M.; Seo, J. E.; Lee, Y.-G.; Lee, S. H.; Cho, K. Y.; Park, J.-K. Effects of triacetoxyvinylsilane as SEI layer additive on electrochemical performance of lithium metal secondary battery. *Electrochem. Solid-State Lett.* **2007**, *10*, A216−A219.

(25) Ota, H.; Shima, K.; Ue, M.; Yamaki, J.-i. Effect of vinylene carbonate as additive to electrolyte for lithium metal anode. *Electrochim. Acta* **2004**, *49*, 565−572.

(26) Zhang, X. Q.; Cheng, X. B.; Chen, X.; Yan, C.; Zhang, Q. Fluoroethylene Carbonate Additives to Render Uniform Li Deposits in Lithium Metal Batteries. *Adv. Funct. Mater.* **2017**, *27*, 1605989.

(27) Xu, W.; Wang, J. L.; Ding, F.; Chen, X. L.; Nasybulin, E.; Zhang, Y. H.; Zhang, J. G. Lithium metal anodes for rechargeable batteries. *Energy Environ. Sci.* **2014**, *7*, 513−537.

(28) Suo, L. M.; Hu, Y. S.; Li, H.; Armand, M.; Chen, L. Q. A new class of Solvent-in-Salt electrolyte for high-energy rechargeable metallic lithium batteries. *Nat. Commun.* **2013**, *4*, 1481.

(29) Liu, Y.; Lin, D.; Yuen, P. Y.; Liu, K.; Xie, J.; Dauskardt, R. H.; Cui, Y. An Artificial Solid Electrolyte Interphase with High Li-Ion Conductivity, Mechanical Strength, and Flexibility for Stable Lithium Metal Anodes. *Adv. Mater.* **2017**, *29*, 1605531.

(30) Han, X.; Gong, Y.; Fu, K. K.; He, X.; Hitz, G. T.; Dai, J.; Pearse, A.; Liu, B.; Wang, H.; Rubloff, G.; et al. Negating interfacial impedance in garnet-based solid-state Li metal batteries. *Nat. Mater.* **2016**, *16*, 572−579.

(31) Huang, J.; Luo, J. A facile and generic method to improve cathode materials for lithium-ion batteries via utilizing nanoscale surface amorphous films of self-regulating thickness. *Phys. Chem. Chem. Phys.* **2014**, *16*, 7786−7798.

(32) Leung, K.; Qi, Y.; Zavadil, K. R.; Jung, Y. S.; Dillon, A. C.; Cavanagh, A. S.; Lee, S.-H.; George, S. M. Using atomic layer deposition to hinder solvent decomposition in lithium ion batteries: first-principles modeling and experimental studies. *J. Am. Chem. Soc.* **2011**, *133*, 14741−14754.




DOI: 10.1021/acs.chemmater.8b01996
*Chem. Mater.* 2018, 30, 5655−5662

(33) Dey, A.; Sullivan, B. The electrochemical decomposition of propylene carbonate on graphite. *J. Electrochem. Soc.* **1970**, *117*, 222−224.
(34) Kozen, A. C.; Lin, C.-F.; Pearse, A. J.; Schroeder, M. A.; Han, X.; Hu, L.; Lee, S.-B.; Rubloff, G. W.; Noked, M. Next-generation lithium metal anode engineering via atomic layer deposition. *ACS Nano* **2015**, *9*, 5884−5892.



DOI: 10.1021/acs.chemmater.8b01996
*Chem. Mater.* 2018, 30, 5655−5662